Food Innovation and Advances

ARTICLE

Open Access

https://doi.org/10.48130/fia-0026-0045

Food Innovation and Advances **2026**, 5(4): 503–517

Broccoli leaf phenolics alleviate NAFLD associated with EGFR/AKT/SREBP signaling regulation and gut microbiota remodeling

Yaqi Zhao[1,2], Wenyuan Zhang[2], Yuanshou Zhao[3], Yue Li[4], Qian Wang[5], Zhanquan Zhang[2], Haixia Yang[5], Liwang Liu[1*] and Jianjun Deng[2*]

[1] *National Key Laboratory of Crop Genetics and Germplasm Enhancement, Key Laboratory of Horticultural Crop Biology and Genetic Improvement (East China) of MOAR, College of Horticulture, Nanjing Agricultural University, Nanjing 210095, China*
[2] *State Key Laboratory of Vegetable Biobreeding, Institute of Vegetables and Flowers, Chinese Academy of Agricultural Sciences, Beijing 100081, China*
[3] *Lanzhou Industry Research Institute, Lanzhou, Gansu 730050, China*
[4] *Haide College, Ocean University of China, Qingdao 266100, China*
[5] *College of Food Science and Nutritional Engineering, China Agricultural University, Beijing 100083, China*
* Correspondence: nauliulw@njau.edu.cn (Liu L); dengjianjun@nwu.edu.cn (Deng J)

Abstract

Broccoli leaves are commonly discarded during industrial processing despite being rich in bioactive phytochemicals, resulting in substantial resource waste. This study investigated the protective effects and potential underlying mechanisms of an ultrasound-assisted green extract of broccoli leaf phenolics (BLP) against high-fat diet (HFD)-induced non-alcoholic fatty liver disease (NAFLD). LC-MS/MS profiling revealed that BLP was predominantly composed of cinnamic acid derivatives and flavonoids, notably sinapic acid, ferulic acid, kaempferol, and luteolin. In HFD-fed C57BL/6J mice, BLP supplementation significantly ameliorated hepatic steatosis and liver injury, as evidenced by reduced serum AST, ALT, and lipid levels, including TG, TC, and LDL. Molecular analyses indicated that BLP suppressed hepatic lipogenesis, accompanied by downregulation of SREBP-1c and modulation of the EGFR/AKT/SREBP signaling pathway. BLP also attenuated inflammatory responses, accompanied by inhibition of the TLR4/NF-κB pathway and reductions in the expression of pro-inflammatory cytokines, including *IL-6*, *IL-1β*, and *TNF-α*. Furthermore, BLP improved intestinal barrier function, as indicated by increased mRNA expression of tight-junction-related genes (*ZO-1*, *Claudin-1*, *Occludin*), and partially restored HFD-associated alterations in gut microbiota composition, particularly affecting genera such as *Lactobacillus* and *Parabacteroides*. Overall, these findings suggest that BLP alleviates HFD-induced NAFLD through coordinated modulation of hepatic lipid metabolism, inflammatory responses, intestinal barrier function, and gut microbiota composition. These effects may involve modulation of the gut-liver axis, highlighting the potential of BLP as a value-added, food-derived functional ingredient for NAFLD prevention.

Keywords: Broccoli leaf phenolics, Non-alcoholic fatty liver disease, Network pharmacology, EGFR/AKT/SREBP pathway, Gut microbiota

Citation: Zhao Y, Zhang W, Zhao Y, Li Y, Wang Q, et al. 2026. Broccoli leaf phenolics alleviate NAFLD associated with EGFR/AKT/SREBP signaling regulation and gut microbiota remodeling. *Food Innovation and Advances* 5(4): 503–517 https://doi.org/10.48130/fia-0026-0045

Introduction

Non-alcoholic fatty liver disease (NAFLD) is a metabolic-related chronic liver disease characterized primarily by abnormal lipid deposition in the liver, also known as metabolic dysfunction-associated steatotic liver disease (MASLD)[1]. Its incidence has been steadily increasing due to the prevalence of obesity and metabolic syndrome, making it one of the most common chronic liver diseases worldwide[2,3]. Currently, clinical intervention for NAFLD mainly relies on lifestyle modifications (such as dietary control and exercise intervention) and drug treatments targeting metabolic disorders such as insulin resistance and dyslipidemia[4]. However, poor long-term adherence, significant individual variability in efficacy, and potential adverse reactions still limit its widespread application. Therefore, developing safe, effective, and suitable novel prevention and treatment strategies for long-term intervention has become an important direction for NAFLD.

Plant extracts and concentrates have recently attracted increasing attention for their potential role in the prevention and treatment of NAFLD. Unlike single-target drugs, plant-derived bioactive compounds exert therapeutic effects through coordinated multi-target regulation, simultaneously modulating hepatic lipid metabolism, inflammatory responses, oxidative stress, and gut–liver axis homeostasis by activating metabolic pathways such as AMPK and PPAR, inhibiting NF-κB-mediated chronic inflammation, and reshaping gut microbiota composition and its metabolites[5–7]. For example, flavonoid-rich mulberry leaf (*Morus*) extract has been shown to effectively alleviate hepatic lipid deposition and inflammatory response in a high-fat diet-induced mice model by improving lipid metabolism, enhancing antioxidant capacity, and regulating gut microbiota structure[8]. Conjugated polyphenols from millet (*Setaria italica*) have been reported to significantly improve NAFLD-related phenotypes by restoring gut microbiota balance, enhancing intestinal barrier function, and reducing hepatic lipid accumulation and inflammation levels[9]. These studies collectively demonstrate that plant extract concentrates can exert anti-NAFLD effects through the synergistic regulation of the gut-liver axis and multiple metabolic and inflammatory signaling pathways, highlighting their potential value as a safe, readily available, and suitable long-term intervention strategy for the prevention and treatment of metabolic diseases.

Broccoli (*Brassica oleracea* var. *italica*), a member of the Cruciferae family, is widely consumed for its rich content of vitamin C, carotenoids, and glucosinolates, which exhibit antioxidant, anti-inflammatory, and potential anticancer activities[10–13]. However, large quantities of leaves and stalks generated during cultivation and processing are typically discarded, leading to substantial resource waste. Our previous study showed that broccoli leaves contain significantly higher levels of flavonoids than florets, while

© The Author(s)

https://doi.org/10.48130/fia-0026-0045

maintaining comparable levels of total phenolics and vitamin C[10]. Among these bioactive constituents, phenolic acids have attracted considerable attention due to their potent antioxidant and antimicrobial properties, conferring broad application potential in the food, pharmaceutical, and cosmetic industries[13]. Major phenolic acids in broccoli include caffeic acid, chlorogenic acid, neochlorogenic acid, ferulic acid, and sinapic acid[14,15]. Despite these advantages, the valorization of broccoli leaves remains underexplored. Therefore, the development of green and efficient extraction strategies, together with systematic evaluation of their bioactivities, is essential to unlock their full potential. Water is an ideal green solvent due to its safety, environmental compatibility, availability, and low cost[11]. However, aqueous extraction processes for broccoli leaves have not yet been systematically optimized for the recovery and characterization of bioactive compounds.

In this study, BLP was selected as the primary focus to investigate its potential health-promoting effects. The phytochemical profile of BLP was comprehensively characterized, and its potential effects on NAFLD were evaluated using preventive and therapeutic mouse models, together with network-pharmacology and molecular-docking analyses. The safety of BLP was first assessed in mice, followed by the establishment of preventive and therapeutic models of high-fat diet (HFD)-induced NAFLD to investigate its effects on serum and hepatic lipid levels, liver injury markers, histopathological changes, inflammatory cytokines, and gut microbiota composition. In addition, a network pharmacology approach was employed to identify potential molecular targets, followed by enrichment analysis and molecular docking to elucidate the underlying mechanisms. This integrated strategy provides a systematic evaluation of the efficacy and mechanistic basis of BLP in alleviating NAFLD.

Materials and methods

Materials

Fresh 'Youxiu' broccoli by-product leaves were collected in June 2024 from the SanJiaoCheng Township, Yuzhong County, Lanzhou City, Gansu Province (China). All chemicals used in this study were UPLC-grade.

Sample preparation

The extraction process of broccoli leaf phenolics (BLP) is illustrated in Supplementary Fig. S1. Fresh broccoli leaves were washed, dried, and pulverized. After cleaning, the leaves were cut into small pieces and evenly distributed on drying trays (Changsheng Machinery Co., Ltd, CS-6CHZ-9), followed by drying at 45 °C for 60 h until the moisture content was below 6%. The Vornoli et al. technique was used to make the water extract[16]. A wall-breaking machine (Zhongshan Huiren Electric Appliance Co., Ltd, 919E) was used to crush the dried leaves before they were put through an 80-mesh sieve. The powder was dispersed in distilled water at 200 mg/mL and ultrasonicated for 1 h at room temperature (KQ-30L, Zhengzhou Yuhua Instrument Manufacturing Co., Ltd) at a frequency of 40 kHz and an ultrasonic power of 600 W, and then stirred on a magnetic stirrer (IKA C-MAG HS7) at 600 rpm for 1 h. The mixture was centrifuged at 4,000 rpm, and the supernatant was collected, stored at −80 °C, and freeze-dried using a vacuum dryer (Boyikang, Pilot 2–4 m, China). The obtained freeze-dried extract powder was used as BLP for subsequent experiments. The total phenolic content of BLP was determined by the Folin–Ciocalteu method and used as a quality control parameter. The dosage used in animal experiments was calculated based on the weight of the freeze-dried extract powder.

Phenolics concentration measurement

The total phenolic content (TPC) of the freeze-dried extract was determined using the Folin–Ciocalteu method. Briefly, the sample was dissolved in distilled water and centrifuged, and 100 μL of the supernatant was mixed with 500 μL of 10-fold diluted Folin–Ciocalteu reagent. After 5 min, 400 μL of sodium carbonate solution (7.5%, w/v) was added, followed by incubation in the dark for 30 min at room temperature. The absorbance was measured at 765 nm. Gallic acid was used to generate the calibration curve (R^2 > 0.99), and the results were expressed as mg gallic acid equivalents per gram of extract (mg GAE/g extract). All measurements were performed in triplicate.

Animal experiments

All animal experiments were approved by the Animal Care and Use Committee of China Agricultural University (AW12106202-5-02). (1) Safety assessment: Eight-week-old male C57BL/6J mice were kept in controlled environments with free access to food and water (22 ± 2 °C, 40%–60% humidity, and a 12-h light/dark cycle). Following a week of acclimatization, mice were divided into two groups at random (n = 4 per group): BLP-treated (800 mg/kg/day BLP, by oral gavage for 7 d) and control (normal chow). Body weight and food consumption were monitored every day for the duration of the treatment[16]. (2) Preventive experiments: Thirty six-week-old male C57BL/6J mice were randomly assigned to five groups (n = 6 per group) after being acclimated to the same conditions: normal (standard chow + 0.2 mL water), model (High-fat diet, HFD + 0.2 mL water, D12492, Research Diets Inc., New Brunswick, NJ, USA), simvastatin (HFD + 10 mg/kg/d simvastatin), low-dose BLP (HFD + 300 mg/kg/d BLP), and high-dose BLP (HFD + 600 mg/kg/d BLP). The HFD contained 5.24 kcal/g energy density, with 60 kcal% fat, 20 kcal% carbohydrate, and 20 kcal% protein. Treatment lasted ten weeks. Body weight was recorded weekly, and food and water intake were measured every 2–3 d[17]. The doses of BLP used in this study were selected based on previous studies investigating the biological activities of plant-derived phenolic extracts and preliminary experiments conducted in our laboratory. The doses of 300 and 600 mg/kg/d were selected to evaluate the dose-dependent protective effects of BLP, while 800 mg/kg/day was applied for safety assessment to evaluate potential toxicity under relatively high exposure conditions. (3) Therapeutic experiments: Another group of tThirty male C57BL/6J mice, aged 6 weeks, was housed under the same conditions, acclimated for one week, and randomly assigned to five groups: normal (standard chow + 0.2 mL water), model (HFD + 0.2 mL water), simvastatin (HFD + 10 mg/kg/d), low-dose BLP (HFD + 300 mg/kg/d), and high-dose BLP (HFD + 600 mg/kg/d). After 14 weeks on their respective diets, mice received the indicated treatments by oral gavage while continuing their respective diets for an additional 14 weeks[18]. At the end of each experiment, mice were fasted for 8 h with free access to water, weighed, and euthanized by retro-orbital blood collection followed by cervical dislocation. Tissues were collected and weighed for further analysis.

Biochemical analysis

As directed by the manufacturer, commercial test kits (Nanjing Jiancheng Bioengineering Institute, Nanjing, China) were used to assess biochemical parameters in the liver and serum of mice. Blood samples were collected and centrifuged to obtain serum, which was

then used for assays. For liver lipid analysis, liver tissue was homogenized, and total lipids were extracted using ethanol extraction. The extracted lipids were then used for assays. Intrahepatic triglyceride (TG) levels were standardized by liver tissue weight and expressed as mg/g liver tissue. Aspartate aminotransferase (AST, No. C010-2-1), alanine aminotransferase (ALT, No. C009-2-1), total cholesterol (TC, No. A111-1-1), Triglyceride (TG, No. A110-1-1), low-density lipoprotein cholesterol (LDL-C, No. A113-1-1), and high-density lipoprotein cholesterol (HDL-C, No. A112-1-1).

Detection of histopathology in mice

After euthanasia, the liver and other tissues were quickly removed and fixed in 4% paraformaldehyde for 24 h. Samples were then embedded in paraffin and cut into 5 μm sections. Hematoxylin and eosin (H&E) staining was used to examine tissue structure. Additional liver samples were embedded in OCT compound, cryosectioned, and stained with Oil Red O to assess lipid accumulation. The area of Oil Red O staining was quantitatively analyzed using Image-Pro Plus 6.0 software. All sections were examined and imaged with a light microscope.

Oral glucose tolerance test (OGTT) and insulin tolerance test (ITT)

To evaluate glucose homeostasis, the BLP intervention experiment conducted oral glucose tolerance tests (OGTT) and insulin tolerance tests (ITT) at weeks eight and nine, respectively, while the BLP treatment experiment carried out oral OGTT and ITT at weeks 12 and 13, respectively. For the OGTT, mice were fasted for 8 h with free access to water. Baseline blood glucose (0 min) was measured from tail vein blood using a standard glucometer. Mice were then orally administered glucose (2 g/kg body weight), and blood glucose levels were recorded at 30, 60, 90, and 120 min post-gavage. For the ITT, following a 6 h fast, mice received an intraperitoneal injection of insulin (1 U/kg body weight), with blood glucose monitored at the same time intervals. The area under the curve (AUC) for both tests was calculated using the standard trapezoidal rule.

16S rRNA gene sequencing and data analysis

A total of six biological replicates per group were analyzed for 16S rRNA gene sequencing. The DNeasy PowerSoil Kit was used to extract total DNA from culture or fecal samples (Qiagen, Hilden, Germany). On a Bio-Rad PCR system, the V3–V4 region of the 16S rRNA gene was amplified using universal primers in 25 μL PCR reactions. Agencourt AMPure XP magnetic beads (Beckman Coulter, USA) were used to purify the PCR products after they were separated by agarose gel electrophoresis. A Qubit dsDNA test kit was then used to quantify the results. OE Biotech Co., Ltd (Shanghai, China) used an Illumina MiSeq platform (Illumina Inc., San Diego, CA, USA) to pool and sequence equimolar amplicons.

Cutadapt was used to eliminate adapters from raw sequencing data (FASTQ). DADA2 in QIIME2 (v2020.11) was used for filtering, denoising, merging, and chimera elimination. The Silva v138 database was used to create amplicon sequence variants (ASVs) and assign taxonomy to representative sequences using the q2-feature-classifier plugin. QIIME2 was used for sequence processing, phylogenetic tree construction, and diversity analyses. Alpha diversity was evaluated using the Chao1 richness and Simpson diversity indices. Beta diversity was assessed based on Bray–Curtis dissimilarity, and principal coordinates analysis (PCoA) was performed to visualize the differences in microbial community composition among groups. Rarefaction curves were generated to evaluate sequencing depth and data coverage. The ASV abundance table generated by DADA2 was normalized based on relative abundance for taxonomic composition analysis. Differentially abundant microbial taxa were identified using linear discriminant analysis effect size (LEfSe). Statistical differences in microbial abundance between groups were determined using the Wilcoxon rank-sum test, and multiple comparisons were corrected using the Benjamini–Hochberg false discovery rate (FDR) method where applicable.

LC-MS/MS analysis

The phenolic composition of broccoli leaf phenolic extract (BLP) was characterized using ultra-high-performance liquid chromatography coupled with high-resolution tandem mass spectrometry (UPLC-QE-HF-MS/MS)[19]. Briefly, 50 mg of freeze-dried BLP powder was dissolved in 0.5 mL of pre-chilled 80% methanol, vortexed thoroughly, and extracted at −20 °C for 30 min. The extraction mixture was subsequently centrifuged at 20,000 × g for 15 min at 4 °C, and the supernatant was collected for LC-MS/MS analysis. Prior to injection, the extracts were filtered through a 0.22 μm membrane filter. Quality control (QC) samples were prepared by mixing equal volumes of individual extracts to monitor analytical stability. An UltiMate 3000 UPLC system (Thermo Fisher) with a T3 column (100 mm × 2.1 mm, 1.8 μm; Waters) was used for the LC-MS analysis at 40 °C. Solvent A (5 mM ammonium acetate and 5 mM acetic acid in water) and solvent B (acetonitrile) were used as mobile phases at a flow rate of 0.3 mL/min. 0–0.8 min, 2% B; 8.0–8.1 min, 100%–2% B; 8.1–10.0 min, 2% B. Mass spectrometric analysis was conducted using a Q-Exactive high-resolution mass spectrometer (Thermo Scientific) equipped with an electrospray ionization source operated in both positive and negative ion modes. Full MS spectra were acquired at a resolution of 70,000 with an automatic gain control (AGC) target of 3×10^6 over an m/z range of 70–1,050. MS/MS spectra were collected using a data-dependent acquisition mode at a resolution of 17,500. Phenolic compounds were identified based on accurate molecular mass, MS/MS fragmentation patterns, and comparison with authentic standards or public databases. The relative abundance of the identified phenolic compounds was estimated based on their relative peak areas, calculated as the peak area of each compound divided by the sum of the peak areas of all identified phenolic compounds, and expressed as a percentage (%). Because authentic standards and calibration curves were not available for all identified compounds, these values represent semi-quantitative relative abundances rather than absolute concentrations.

Network pharmacology and molecular docking

We estimated the active components and important targets of BLP using previously reported methods[20]. Potential active molecules of BLP were found using SwissTargetPrediction (www.swisstargetprediction.ch/) and the TCMSP database (https://old.tcmsp-e.com/tcmsp.php). The SMILES structures required for SwissTargetPrediction were supplied by PubChem (https://pubchem.ncbi.nlm.nih.gov). Using the phrase 'NAFLD,' GeneCards (www.genecards.org), OMIM (https://omim.org), and TTD (https://idrblab.net/ttd) provided illness-related targets for nonalcoholic fatty liver disease (NAFLD). After gathering all of the targets, duplicates were removed. The overlapping targets between BLP and NAFLD were visualized using a Venn diagram (www.liuxiaoyuyuan.cn). The DAVID database (https://davidbioinformatics.nih.gov/summary.jsp) was used for the Kyoto Encyclopedia of Genes

https://doi.org/10.48130/fia-0026-0045

and Genomes (KEGG) and Gene Ontology (GO) enrichment studies. A compound–target–pathway network was constructed using the active compounds, relevant targets, and enriched pathways. Overlapping targets were further investigated by building a protein–protein interaction (PPI) network using STRING 11.5 (https://string-db.org). The CentiScape 2.2 plugin in Cytoscape 3.9.1 was used to perform topological analysis of the PPI network in order to identify key genes.

Molecular docking was used to investigate the binding affinity and interaction processes between possible bioactive chemicals in BLP and important targets found by network pharmacology. The chemicals were docked with anticipated target proteins using AutoDock Vina 1.1.2. The AlphaFold database (https://alphafold.ebi.ac.uk) provided the protein structures, which were preprocessed in PyMOL 2.4 by adding hydrogen atoms and removing water molecules and hetero-ligands. ChemDraw 20.0 (PerkinElmer, Waltham, MA, USA) was used to decrease the energy of compound structures before converting them to PDBQT format for docking. Other settings were left at their default values, and the docking grid encompassed the whole protein structure. Nine binding conformations were produced for every compound-target combination; the conformation with the highest frequency and lowest binding energy was regarded as the most likely binding mode. Docking results were visualized using PyMOL 2.4.

RNA extraction and real-time quantitative PCR (RT-qPCR)

The TRIzol reagent (TIANGEN, Beijing, China) was used to extract total RNA from 30 mg colon tissue and 30 mg liver tissue. Using a first-strand cDNA synthesis kit (TIANGEN, Beijing, China), 1 μg of RNA was converted into first-strand cDNA. The $2^{-\Delta\Delta CT}$ technique was used to calculate the levels of gene expression. Supplementary Table S1 lists the sequences of the primers that were acquired from Qingke Company.

Western blot

In accordance with previously published procedures[21], liver tissue and colon tissue were collected and homogenized in ice-cold RIPA lysis solution supplemented with a 1% phosphatase and protease inhibitor cocktail. The protein concentration was determined using a bicinchoninic acid (BCA) protein assay kit (Solarbio, Beijing, China; Cat. No. PC0020-50T). Equal amounts of total protein (30 μg per lane) were separated on 4%–20% SDS–PAGE gels and transferred onto 0.22 μm PVDF membranes (Millipore, Billerica, MA, USA). After blocking, the membranes were incubated with primary antibodies against EGFR (1:750, No. GB151504-50), p-EGFR (1:750, No. GB115662-50), AKT (1:1500, No. GB15689-50), p-AKT (1:1500, No. GB150002-50), PI3K (1:1000, No. GB113360-50), SREBP-1c (1:750, No. GB113804-50), NF-κB (1:750, No. GB15997-50), p-p65 (1:400, No. GB153882-50), and TLR4 (1:750, No. GB15519-50). All primary antibodies were purchased from Servicebio (Wuhan, China). GAPDH (1:4000, Cat. No. GB15002-100, Servicebio, Wuhan, China) was used as the loading control for normalization. The membranes were subsequently incubated with HRP-conjugated goat anti-rabbit IgG secondary antibody (1:5,000) for 45 min at room temperature. Protein bands were visualized using an enhanced chemiluminescence (ECL) detection kit (Wuhan Aibotek Biotechnology Co., Ltd), and images were captured using a Bio-OI imaging system (OI600, Guangzhou Guangyi Biotechnology Co., Ltd). ImageJ software (NIH, Bethesda, MD, USA) was used to quantify band intensities.

Statistical analysis

R software (v4.2.2) was used to conduct bioinformatics studies. SPSS 23.0 (IBM, Armonk, NY, USA) was used for statistical analysis, and OriginPro 2021 (OriginLab, Northampton, MA, USA) was used for data visualization. Data are presented as mean ± standard deviation (SD). For comparisons among multiple groups, normally distributed data with homogeneous variance were analyzed using one-way analysis of variance (ANOVA) followed by Tukey's multiple comparisons test. A p-value < 0.05 was considered statistically significant.

Results and discussion

BLP extraction and characterization

The extraction process of BLP is illustrated in Supplementary Fig. S1. A comprehensive LC-MS/MS analysis of broccoli leaf extract identified 24 phenolic compounds (Table 1), predominantly comprising cinnamic acids, flavonoids, and coumarins. Cinnamic acid derivatives constitute the primary phenolic group, with sinapic acid and ferulic acid accounting for over 28% of the total profile, accompanied by significant levels of valuable flavonoids, particularly kaempferol and luteolin. These findings align with the typical phenolic profile of Brassica vegetables[22]. In addition, the total phenolic content of the extract, determined by the Folin–Ciocalteu method, was 10–14 mg GAE/g extract, providing quantitative support for the relative abundance observed in the LC–MS/MS analysis. Notably, the substantial accumulation of both free and conjugated sinapic acid in the foliage indicates highly conserved secondary metabolite biosynthetic pathways compared to the widely studied edible florets[23]. Furthermore, high-resolution profiling facilitated the precise detection of minor glycosylated flavonoids and anthocyanins[24], reflecting adaptive defense mechanisms against environmental stressors[25]. While some literature identifies chlorogenic acid as the major broccoli phenolic[26], the present dataset revealed a relatively higher abundance of coumarins, such as bergaptol, which may be attributed to genotypic or environmental variation. Notably, an ultrasound-assisted aqueous extraction strategy was employed to obtain broccoli leaf phenolic extracts, providing a practical approach for recovering bioactive phenolic compounds from broccoli leaf by-products. Overall, these results provide a comprehensive characterization of the phenolic composition of broccoli leaves and suggest that this underutilized biomass may serve as a promising and sustainable source of bioactive compounds with potential for value-added applications[27–28].

The effect of BLP on NAFLD in mice

Assessing the safety of BLP

To preliminarily evaluate the safety of BLP before investigating its metabolic benefits, mice were administered BLP at a high dose (800 mg/kg/d) for 7 d, and body weight, organ coefficients, and histological changes were assessed. Therefore, a relatively high dose of BLP (800 mg/kg/d) was selected for preliminary safety evaluation based on previous studies of plant-derived bioactive extracts, allowing assessment of potential adverse effects under excessive exposure conditions[29]. BLP was evaluated for toxicity and obesity-preventive effects in C57BL/6J mice. In the toxicity study (Fig. 1a), oral administration of BLP at 800 mg/kg caused no significant changes in body weight or in the weights of major organs (heart, spleen, lung, kidney, and brain) compared with the normal group

Table 1. Phenolic compounds identified in broccoli leaf by LC-MS/MS.

No.	Compound name	Formula	Class	Content (%)
1	3-(2-hydroxyphenyl)propanoic acid	C9H10O3	Phenylpropanoic acids	0.45
2	Kaempferol	C15H10O6	Flavonoids	9.86
3	Luteolin	C15H10O6	Flavonoids	9.21
4	Astragalin	C21H20O11	Flavonoids	4.35
5	Cyanidin	C15H11O6	Flavonoids	2.19
6	Kaempferol 3-gentiobioside	C27H30O16	Flavonoids	1.25
7	Cyanidin-3,5-diglucoside	C27H31O16	Flavonoids	1.25
8	Cyanidin 3-galactoside	C21H21O11	Flavonoids	1.07
9	Kaempferol 3-O-[2″-O-(E)-feruloylgalactosyl-(1→4)-glucoside]	C37H38O19	Flavonoids	0.8
10	3-Hydroxyflavone	C15H10O3	Flavonoids	0.58
11	Bergaptol	C11H6O4	Coumarins and derivatives	5.89
12	Umbelliferone	C9H6O3	Coumarins and derivatives	2.1
13	6-Formylumbelliferone	C10H6O4	Coumarins and derivatives	1.46
14	Aesculetin	C9H6O4	Coumarins and derivatives	0.57
15	Scopoletin	C10H8O4	Coumarins and derivatives	0.42
16	Sinapic acid	C11H12O5	Cinnamic acids and derivatives	14.45
17	Ferulic acid	C10H10O4	Cinnamic acids and derivatives	13.55
18	Caffeic acid	C9H8O4	Cinnamic acids and derivatives	6.43
19	1-O-Sinapoyl-β-D-glucose	C17H22O10	Cinnamic acids and derivatives	5.11
20	Isoferulic acid	C10H10O4	Cinnamic acids and derivatives	5
21	4-Hydroxycinnamic acid	C9H8O3	Cinnamic acids and derivatives	4.21
22	*trans*-Cinnamic acid	C9H8O2	Cinnamic acids and derivatives	3.52
23	2-Hydroxycinnamic acid	C9H8O3	Cinnamic acids and derivatives	2.18
24	p-Coumaraldehyde	C9H8O2	Cinnamaldehydes	4.08

($p > 0.05$) (Fig. 1b, c). Histological analysis further confirmed biocompatibility, as the liver, kidney, and spleen of treated mice showed intact structures, similar to the normal group, indicating no acute toxicity (Fig. 1d). These results indicate that short-term BLP administration at 800 mg/kg/d did not induce obvious toxic effects under the evaluated conditions. However, given the limited sample size, short intervention duration, and available safety parameters, further long-term and comprehensive toxicological studies are required to fully establish the safety profile of BLP. These results confirmed that BLP exhibited good biocompatibility, which is consistent with previously published studies. Previous investigations have shown that 21-d oral administration of broccoli by-product powder in mice does not induce physiological abnormalities or hepatotoxicity[30]. In addition, hydrophilic extracts derived from broccoli by-products have been reported to be safe and to possess functional potential, supporting their applicability as functional food ingredients[31]. Moreover, broccoli seed extracts have been demonstrated to cause neither acute nor sub-chronic toxicity, further reinforcing the low-toxicity profile of broccoli-derived bioactive fractions[32]. Taken together, these studies provide a solid toxicological basis for the subsequent evaluation of the therapeutic efficacy of BLP in metabolic disease models.

The preventive effect of BLP on NAFLD in mice

To further assess the preventive effects of BLP on NAFLD, mice were administered BLP concomitantly with a high-fat diet for ten weeks (Fig.1e). In the HFD-induced NAFLD model, BLP produced a dose-dependent protective effect. All tested doses significantly reduced excessive body-weight gain compared with the Model group ($p < 0.05$) (Fig. 1f). Kidney and brain weight ratios were markedly altered in the Model group relative to the Normal group, whereas BLP treatment partially restored these indices ($p < 0.05$) (Fig. 1g, h). Excessive weight gain and ectopic fat accumulation are major risk factors for NAFLD, primarily leading to increased hepatic lipid deposition[33]. For adipose tissue distribution (Fig. 1i), the fat weight ratios of inguinal white adipose tissue (iWAT), epididymal white adipose tissue (eWAT), and retroperitoneal white adipose tissue (rWAT) were significantly increased in the model group compared with the normal group ($p < 0.05$). BLP treatment reduced fat weight ratios in a dose-dependent manner, with the strongest effect observed in eWAT. Glucose metabolism disorders, particularly insulin resistance, are key drivers of NAFLD progression and exacerbate hepatic glucolipotoxicity[34]. Glucose homeostasis was evaluated using the oral glucose tolerance test (OGTT) and insulin tolerance test (ITT) (Fig. 1j, k). Compared with the model group, BLP-treated mice ameliorated glucose intolerance and insulin resistance ($p < 0.05$). OGTT and ITT curves showed smaller glycemic excursions, indicating better maintenance of glucose homeostasis.

Dyslipidemia is closely linked to the onset and progression of NAFLD, and abnormal serum enzyme activities indicate liver injury[34]. As shown in Fig. 2a–c, serum triglyceride (TG), total cholesterol (TC), and low-density lipoprotein cholesterol (LDL-C) levels were significantly increased in the model group. However, serum HDL-C levels remained comparable between the Model group and all treatment groups (Fig. 2d). Both BLP and simvastatin treatments reduced these lipid levels, with the high-dose BLP group showing the strongest effect ($p < 0.05$). Serum aspartate aminotransferase (AST) and alanine aminotransferase (ALT) activities were markedly elevated in the model group ($p < 0.05$) (Fig. 2e, f), whereas BLP-treated groups significantly lowered ALT and AST, indicating improved liver function. Gross liver morphology revealed clear hepatomegaly and discoloration in the model group (Fig. 2f). Histological analysis using H&E and Oil Red O staining showed severe hepatic steatosis in the model group, while BLP and simvastatin treatment markedly reduced lipid droplet accumulation (Fig. 2h, i). The liver weight ratio (Fig. 2g) and hepatic lipid contents (TC, TG, and LDL-C) were also significantly decreased by BLP treatment ($p < 0.05$) (Fig. 2j–l). During the development of NAFLD, pro-inflammatory factors are released simultaneously[35]. Indeed, we found the proinflammatory cytokines *including interleukin-1β* (*IL-1β*), *tumor necrosis factor-α* (*TNF-α*), and *interleukin-6* (*IL-6*) were strongly upregulated in the model group (Fig. 2m), but were significantly

https://doi.org/10.48130/fia-0026-0045

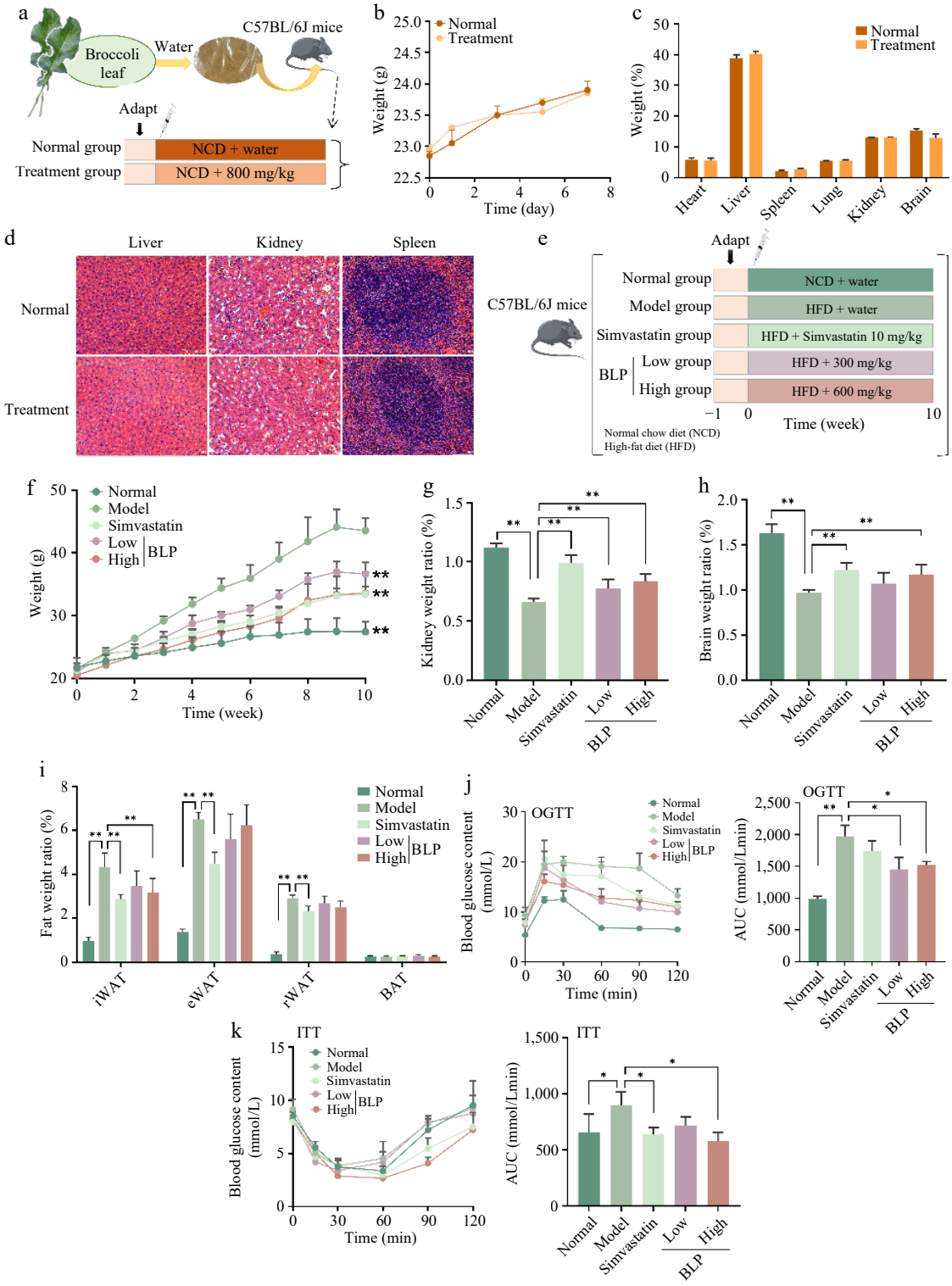


Fig. 1 Experimental design, safety assessment, and preventive effects of BLP in mice. (a) Schematic illustration of the experimental design for safety assessment. (b) Change in body weight. (c) Organ weight percentages. (d) H&E staining of liver, kidney, and spleen tissues, and the scale bar in the lower right corner is 100 μm. (e) Schematic of the experimental design for preventive experiments. (f) Body weight changes over ten weeks, and ** indicates a significant difference ($p < 0.01$) compared with all groups and the model group in the 10th week. (g) Kidney weight ratio. (h) Brain weight ratio. (i) Fat weight ratios of iWAT, eWAT, rWAT, and BAT. (j) OGTT results and area under the curve (AUC). (k) ITT results and AUC. Body weight changes, OGTT, and ITT data were analyzed using two-way repeated-measures ANOVA, considering both treatment groups and time points as variables, followed by appropriate multiple comparisons. *$p < 0.05$, **$p < 0.01$. iWAT, inguinal white adipose tissue; eWAT, epididymal white adipose tissue; rWAT, retroperitoneal white adipose tissue; BAT, brown adipose tissue. OGTT, oral glucose tolerance test; ITT, insulin tolerance test.

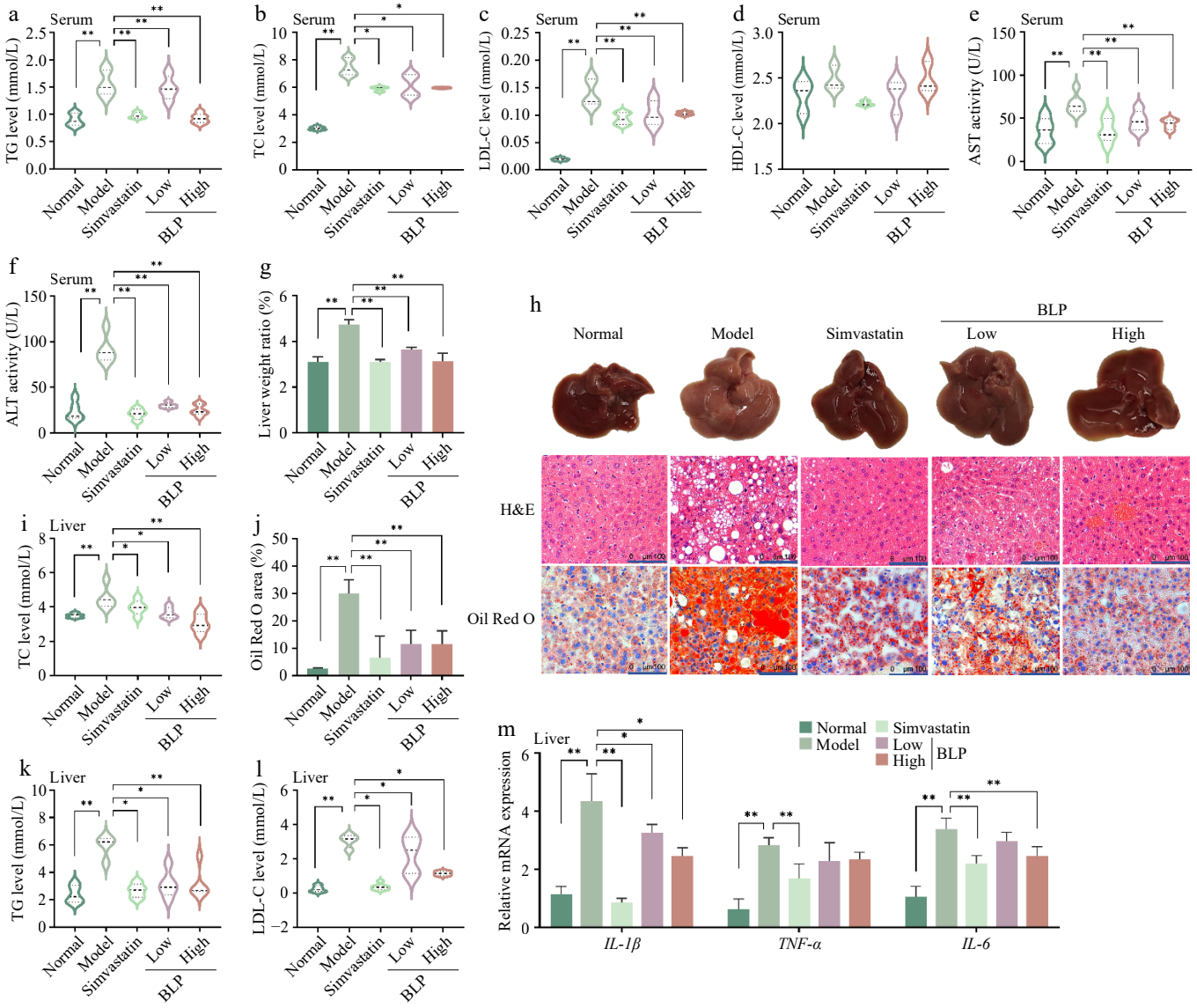


Fig. 2 BLP regulates serum and hepatic lipid profiles and reduces liver inflammation in HFD - induced NAFLD mice. Serum levels of (a) TG, (b) TC, (c) LDL-C, and (d) HDL-C. (e), (f) Serum AST and ALT activities. (g) Liver weight ratio. (h) Representative images of livers and H&E/Oil red O staining. The scale bar at the lower right corner is 100 μm. (i) Quantitative results of Oil Red O staining. Hepatic (j) TG, (k) TC, and (l) LDL-C levels. (m) Relative mRNA expression of pro-inflammatory cytokines (*IL-1β*, *TNF-α*, *IL-6* genes) in the liver. Data are presented as mean ± SD or median with interquartile range ($n = 6$). Statistical significance was determined by one-way ANOVA followed by Tukey's multiple comparisons test. * $p < 0.05$, ** $p < 0.01$. TG, triglyceride; TC, total cholesterol; LDL-C, low-density lipoprotein cholesterol; *IL-1β*, *interleukin-1 beta*; *TNF-α*, *tumor necrosis factor alpha*; *IL-6*, *interleukin-6*.

suppressed by BLP treatment ($p < 0.05$), confirming its anti-inflammatory and hepatoprotective effects[36]. Overall, these results indicate that BLP effectively alleviates HFD-induced NAFLD and associated metabolic disturbances. BLP reduces excessive weight gain and modulates adipose tissue distribution, lowering peripheral drivers of hepatic lipid accumulation. It improves glucose tolerance and insulin sensitivity, relieving metabolic stress on the liver, while correcting dyslipidemia and reducing hepatic enzyme leakage. Importantly, BLP downregulates proinflammatory cytokine expression, providing strong evidence for its anti-inflammatory and liver-protective properties.

The therapeutic potential of BLP on NAFLD in mice

To investigate the therapeutic potential of BLP in a high-fat diet–induced NAFLD model, mice were fed a high-fat diet for 14 weeks to establish NAFLD, followed by BLP treatment for an additional 14 weeks (Fig. 3a). Compared with the normal group, the model group (HFD) exhibited significant body weight gain, whereas BLP-treated groups (Low and High) and the simvastatin group showed varying degrees of inhibition of weight gain ($p < 0.05$), which was consistent with the results observed in the NAFLD prevention experiment (Fig. 3b). Body weight regulation is crucial for metabolic health, as excessive weight gain is a key risk factor for NAFLD, and interventions that limit weight gain often improve metabolic homeostasis[37]. For glucose homeostasis, ITT results indicated that the model group developed insulin resistance, while treatment groups enhanced insulin sensitivity, as reflected by greater reductions in blood glucose following insulin injection (Fig. 3c). OGTT results showed elevated blood glucose in the model group at all time points ($p < 0.05$), whereas BLP treatment improved glucose tolerance, with lower glucose levels at 30, 60, 90, and 120 min ($p < 0.05$) (Fig. 3d). Impaired glucose tolerance and insulin

https://doi.org/10.48130/fia-0026-0045

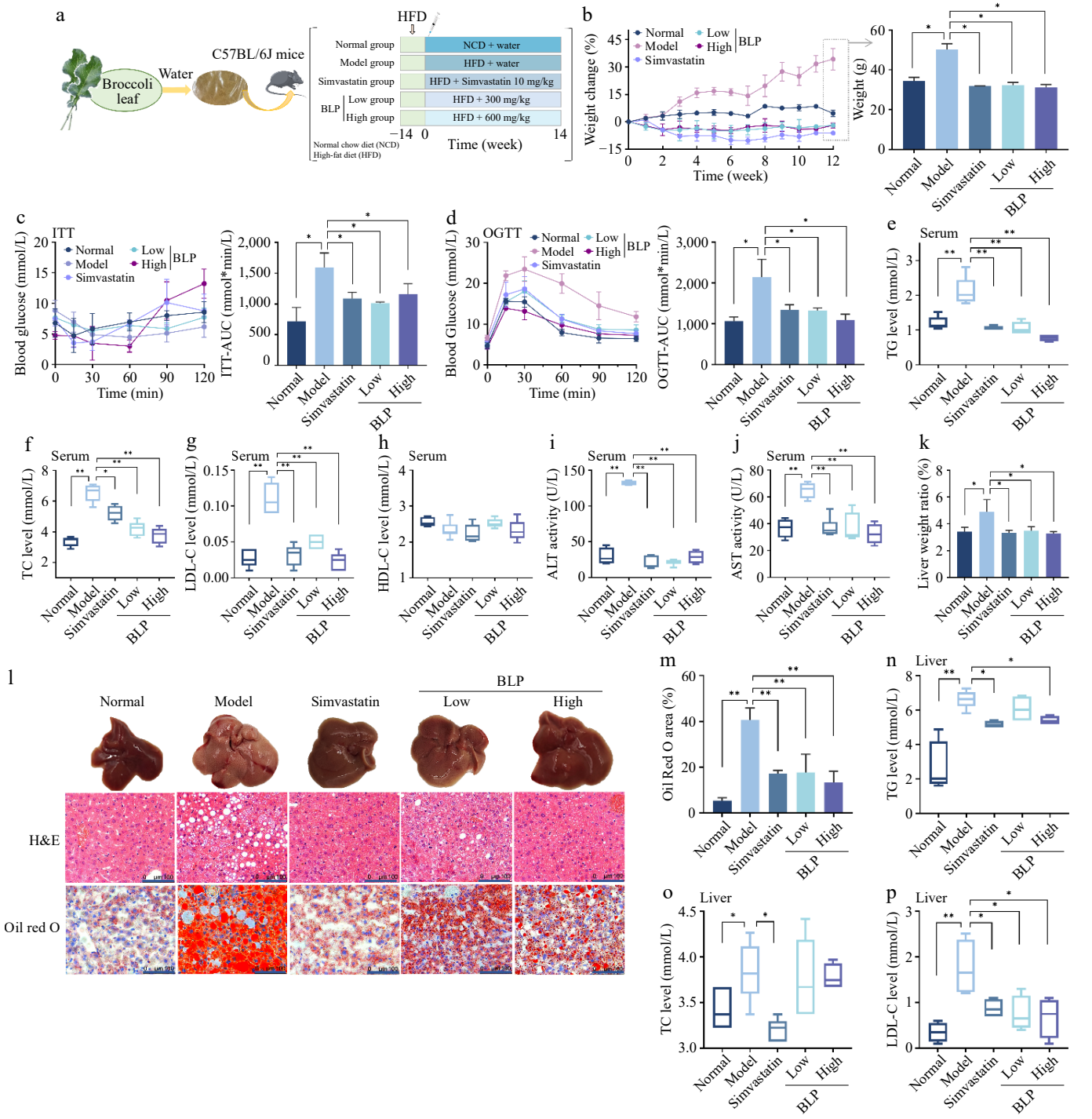


Fig. 3 Therapeutic effects of BLP on body weight, glucose metabolism, and therapeutic regulation in HFD-induced NAFLD mice. (a) Schematic of the therapeutic experimental design. (b) Percentage change in body weight over 14 weeks. (c) ITT and AUC results. (d) OGTT and AUC results. Serum (e) TG, (f) TC, (g) LDL-C, and (h) HDL-C levels. (i), (j) Serum ALT and AST activities. (k) Liver weight ratio. (l) Representative liver images and H&E/oil red O staining, and the scale bar in the lower right corner is 100 μm. (m) Quantitative results of Oil Red O staining. Hepatic (n) TG, (o) TC, and (p) LDL-C levels. Data are presented as mean ± SD or median with interquartile range (n = 6). Statistical significance was determined by one-way ANOVA followed by Tukey's multiple comparisons test. * $p < 0.05$, ** $p < 0.01$.

resistance are central to NAFLD pathogenesis, promoting hepatic lipid accumulation and metabolic dysfunction[38]. The improvement in these parameters by BLP suggests its potential to target key metabolic defects in NAFLD.

In serum lipid profiles, the model group showed significantly higher TG, TC, and LDL-C levels compared with the normal group ($p < 0.01$), indicating HFD-induced dyslipidemia (Fig. 3e–g). However, serum HDL-C levels did not differ significantly among the treatment groups (Fig. 3h). In addition, serum AST and ALT activities were markedly increased, suggesting hepatic injury (Fig. 3i, j). Both simvastatin and BLP treatments (Low and High doses) significantly reduced these indicators, with the high-dose BLP group

approaching normal levels, indicating dose-dependent improvements in lipid metabolism and liver function. Gross liver morphology revealed severe hepatomegaly and pale coloration in HFD-fed mice, whereas BLP-treated mice showed visibly improved liver appearance (Fig. 3l). Histological analyses corroborated these findings: H&E staining revealed substantial lipid droplet accumulation and hepatocellular ballooning in the HFD group, which were alleviated by BLP, while Oil Red O staining demonstrated significant reductions in hepatic lipid deposition in BLP-treated mice (Fig. 3l, m). Liver function assessments showed that the Model group had higher liver weight ratios ($p < 0.05$) (Fig. 3k) and elevated intrahepatic TG, TC, and LDL-C levels ($p < 0.05$) (Fig. 3n–p), consistent with the severe histological changes. Collectively, these results indicate that BLP supplementation effectively mitigates HFD-induced obesity, hyperlipidemia, hyperglycemia, and hepatic steatosis. These bacterial alterations were associated with the metabolic improvements observed after BLP supplementation, which may be related to the bioactive phytochemicals present in BLP and their potential effects on lipid and glucose metabolism, antioxidant defense, and hepatic lipid accumulation. Collectively, these findings demonstrate the protective effects of BLP against NAFLD and highlight its potential as a dietary intervention for the prevention and management of metabolic disorders. Collectively, these findings demonstrate the protective effects of BLP against NAFLD and highlight its potential as a dietary intervention for the prevention and management of metabolic disorders. Although the administered doses were higher than typical dietary exposure levels, they are within the dose range commonly used for evaluating the efficacy and safety of plant-derived bioactive compounds in preclinical studies. Further studies are required to determine the effective human intake levels of BLP. Based on these *in vivo* findings, the prevention group was selected for further mechanistic studies.

Mechanistic investigation of BLP in improving NAFLD

Investigate potential active compounds using network pharmacology

To explore and predict the potential molecular targets underlying the effects of BLP on NAFLD, 24 phenolic metabolites identified through LC-MS/MS analysis were subjected to screening in the Traditional Chinese Medicine Systems Pharmacology Database (TCMSP). The possible targets of these compounds were then predicted using SwissTargetPrediction, yielding a total of 457 targets. In parallel, 3,142 NAFLD-related targets were collected from GeneCards, OMIM, and TTD databases (Fig. 4a). To further investigate the potential mechanisms underlying the therapeutic effects of BLP, we performed bioinformatic analyses. A Venn diagram revealed 134 overlapping targets between BLP phytochemicals and NAFLD-related targets, suggesting potential key mediators of the extract's action (Fig. 4a). Gene Ontology (GO) enrichment analysis (Fig. 4b) showed that these overlapping targets were significantly enriched in biological processes such as signal transduction, protein phosphorylation, and positive regulation of transcription by RNA polymerase II; cellular components including plasma membrane, nucleus, and membrane; and molecular functions such as protein serine/threonine kinase activity, protein kinase activity, and enzyme binding. This pattern is consistent with previous NAFLD studies. Previous studies have shown that disease-relevant genes are enriched in signal transduction, membrane and nuclear compartments, and kinase-related functions, supporting the biological relevance of our findings[39]. KEGG pathway analysis (Fig. 4c) indicated that these targets were involved in multiple signaling pathways, with the PI3K–AKT signaling pathway, lipid and atherosclerosis pathway, and Alzheimer disease pathway being the most significantly enriched. The protein–protein interaction (PPI) network (Fig. 4d) further visualized interactions among key targets and highlighted core proteins that may play central roles in mediating the biological effects of BLP. These bioinformatic results provide insights into the potential molecular mechanisms of BLP in ameliorating HFD-induced NAFLD. The overlap between phytochemical targets and disease-related targets suggests that BLP acts by modulating specific molecular nodes involved in NAFLD pathogenesis. Enrichment in GO terms related to signal transduction and protein phosphorylation implies that BLP may regulate intracellular signaling cascades essential for metabolic control and cell function. Notably, the PI3K–AKT pathway, a central regulator of cell growth, survival, and metabolism, is closely linked to insulin resistance and hepatic lipid accumulation, key features of NAFLD[40,41]. Modulation of this pathway by BLP may improve insulin sensitivity and reduce hepatic steatosis. Furthermore, enrichment in the lipid and atherosclerosis pathway aligns with the observed reductions in serum lipid levels *in vivo*. The PPI network identifies core proteins that may serve as pivotal nodes in BLP-mediated molecular interactions, providing promising targets for further mechanistic studies.

Research on the mechanism of BLP regulating the EGFR/AKT/SREBP pathway

To elucidate the mechanism by which BLP alleviates HFD-induced NAFLD, molecular docking was conducted between its top ten abundant compounds and key PI3K-AKT pathway targets (Fig. 4e). Among them, kaempferol exhibited the strongest binding affinity to AKT1 (−11.0 kcal/mol) and EGFR (−10.9 kcal/mol) (Fig. 4f). Structural visualization revealed that kaempferol may interact with AKT1 (e.g., Thr-101, Asn-53, Trp-21) and EGFR (e.g., Gln-677) through potential hydrogen bonds and hydrophobic interactions (Fig. 4f). This binding mode indicates possible involvement of these proteins in the biological effects of BLP, aligning with kaempferol's known ability to reduce intracellular lipid deposition via the PI3K-AKT pathway. Additionally, other bioactive compounds in BLP, such as luteolin and astragalin, also displayed strong affinities for AKT1 and EGFR. Given that AKT1 and EGFR dysregulation drives hepatic steatosis and inflammation, these network and docking analyses collectively suggest that the EGFR–PI3K–AKT–SREBP-1c pathway may represent a potential signaling mechanism involved in the effects of BLP.

Subsequently, the molecular basis of the preventive effect of BLP on hepatic lipid metabolism was examined. The transcription and protein levels of the EGFR/AKT/SREBP signaling pathway (Fig. 5a) were measured by RT-qPCR and Western blotting. RT-qPCR analysis of mice liver tissue showed that the Model group had higher mRNA expression of *EGFR* and *AKT1* than the Normal group (Fig. 5b, f). However, BLP and simvastatin treatment reduced their expression to near-normal levels. In addition, the transcripts of the *EGFR–AKT* cascade (*PI3K* and *IRS1* genes) were also upregulated in the model group (Fig. 5d, e). The expression of *SREBP-1c* and its adipogenic target genes was increased as well (Fig. 5g, h). These results were consistent with the activation of *de novo* lipogenesis at the early stage of pathology. Furthermore, Western blotting confirmed that the model group showed higher protein levels of phosphorylated EGFR (p-EGFR) and phosphorylated AKT (p-AKT) (Fig. 5i and Supplementary Fig. S2). The PI3K and SREBP-1c protein levels were also elevated, indicating activation of the EGFR–PI3K–AKT–SREBP-1c pathway. In contrast, BLP intervention reduced p-AKT and SREBP-1c levels, while total AKT remained unchanged (Fig. 5j–o). Thus, the

https://doi.org/10.48130/fia-0026-0045

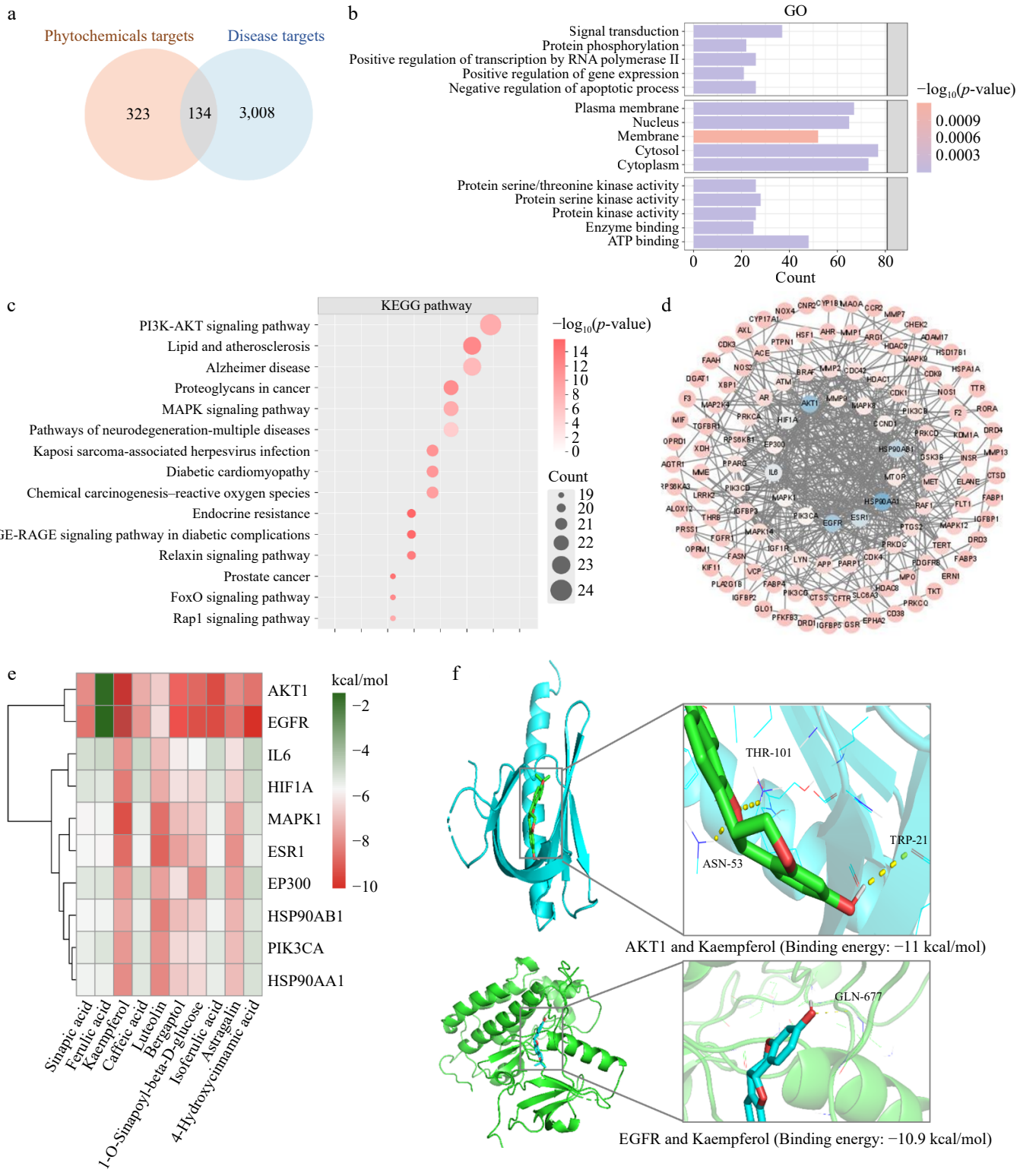


Fig. 4 Integrated bioinformatic and molecular docking analyses reveal key targets of BLP in NAFLD. (a) Venn diagram showing overlapping targets between BLP phytochemicals and NAFLD-associated genes. (b) GO enrichment analysis highlighting biological processes (signal transduction, protein phosphorylation), cellular components (plasma membrane, nucleus), and molecular functions (protein kinase activity, enzyme binding). (c) KEGG pathway analysis showing significant enrichment in PI3K-AKT signaling, lipid metabolism, and other NAFLD-related pathways. (d) PPI network of core targets, illustrating key molecular interactions. (e) Heatmap of binding energies between BLP phytochemicals and potential NAFLD targets. (f) Molecular docking predicted potential interactions between kaempferol and AKT1/EGFR.

regulatory effect of BLP was mainly achieved by blocking phosphorylation-dependent activation rather than by lowering AKT protein abundance. These molecular changes were associated with reduced hepatic lipid deposition, suggesting suppression of lipid production. Furthermore, it is noteworthy that AKT not only acts as a linker growth factor regulating lipid metabolism but also serves as a

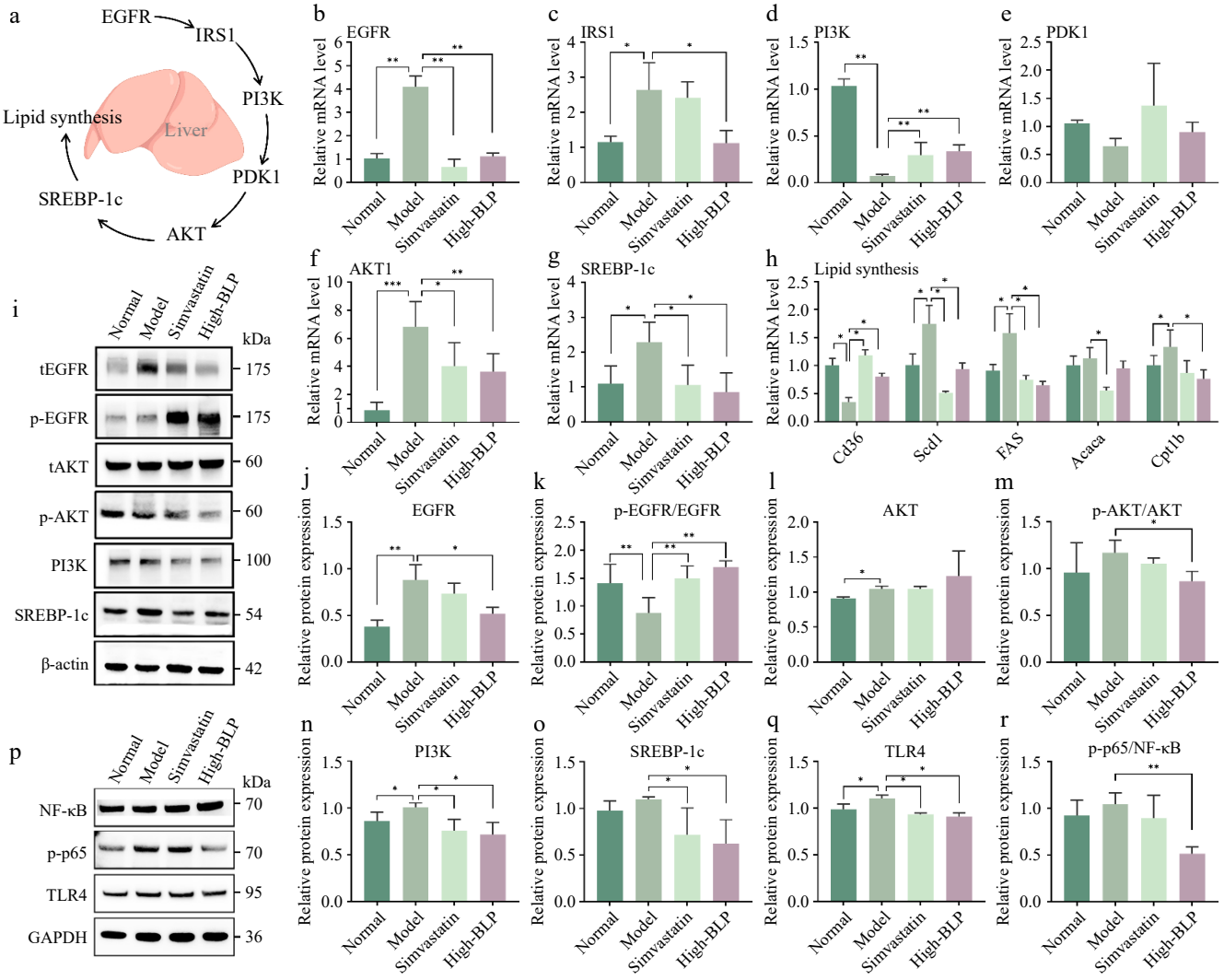


Fig. 5 (a) Schematic diagram of the EGFR/PI3K/AKT/SREBP-1c signaling axis regulating hepatic lipid synthesis. Relative mRNA levels of (b) *EGFR*, (c) *IRSI*, (d) *PI3K*, (e) *PDK1*, (f) *AKT1*, and (g) *SREBP-1c* in mice liver tissues. (h) Relative mRNA levels of lipogenic genes in liver tissues. (i) Representative Western blot bands of tEGFR, p-EGFR, tAKT, p-AKT, PI3K, SREBP-1c, and GAPDH. tEGFR, total EGFR; p-EGFR, Phosphorylated EGFR; tAKT, total AKT; p-AKT, Phosphorylated AKT; Relative protein expression (or phosphorylation ratio) of (j) EGFR, (k) p-EGFR/EGFR, (l) AKT, (m) p-AKT/AKT, (n) PI3K, and (o) SREBP-1c in liver tissues. Western blot bands of (p) NF-κB, p-p65, and TLR4 in liver tissues and (q) quantitative analysis of p-p65/NF-κB and (r) TLR4 in liver tissues. Data are presented as mean ± SD ($n = 6$ per group). Statistical significance was determined by one-way ANOVA followed by Tukey's multiple comparisons test. * $p < 0.05$, ** $p < 0.01$.

central signaling node in the inflammatory response[42]. TLR4 can activate HFD-induced liver inflammation, further enhancing PI3K-AKT signaling[43]. In mouse liver, the model group showed upregulation of TLR4 and p-p65/NF-κB expression ($p < 0.05$), while simvastatin and BLP significantly inhibited these upregulations ($p < 0.05$ and $p < 0.01$) (Fig. 5p–r). This is similar to previous results, where many natural compounds often simultaneously regulate both hepatic lipid metabolism and inflammatory signaling pathways. For example, compounds such as berberine and flavanones from citrus extracts can simultaneously inhibit PI3K-AKT-related lipid metabolism signaling pathways and suppress TLR4/NF-κB activation to alleviate metabolic inflammation[42,44]. Overall, the data highlighted the specific molecular targets and regulatory pattern of potential bioactive components in BLP in NAFLD. BLP showed regulatory effects similar to simvastatin, supporting its potential as a natural treatment for NAFLD. Nevertheless, interactions among multiple phytochemicals in BLP and the network of NAFLD-related targets remain to be clarified. Future studies should investigate the potential synergistic effects among these compounds and validate the roles of key targets such as AKT1 and EGFR. Moreover, the biological effects of dietary phenolic compounds are influenced by their bioavailability and metabolic transformation. Major phenolics identified in BLP, including kaempferol, luteolin, ferulic acid, and sinapic acid, may undergo phase II metabolism and gut microbial transformation after ingestion. Therefore, the docking results should be interpreted as predictive evidence of potential interactions rather than confirmation of *in vivo* mechanisms. Further pharmacokinetic studies are required to determine the bioactive forms responsible for the metabolic benefits of BLP.

Effect of BLP on gut microbiota, intestinal barrier function and inflammation

The role of gut microbiota in regulating NAFLD through the gut–liver axis has received increasing attention[45]. The gut microbiota plays a key role in the development and progression of NAFLD through multiple mechanisms, including increased energy

https://doi.org/10.48130/fia-0026-0045

harvesting, altered intestinal barrier function, and production of metabolites[46]. To investigate the impact of BLP treatments on microbial community composition and structure, 16S rRNA sequencing of fecal samples from three groups of mice was performed. Principal coordinate analysis (PCoA) based on Bray–Curtis dissimilarity (Fig. 6a) revealed clear separation of the microbial communities among the normal, model, and high-dose groups, with PC1 and PC2 explaining 35.63% and 10.47% of the variation, respectively. Notably, the high-dose group was positioned between the normal and model groups, suggesting that BLP could partially reshape gut microbiota composition[47]. The Simpson index reflects the microbial diversity of the gut microbiota, describing how evenly species are distributed. The Chao1 index estimates species richness, indicating the total number of bacterial species. Together, these indices describe the overall structure of the gut microbial community[48]. As shown in Fig. 6b, the Simpson index was significantly reduced in the model group compared with the normal group ($p < 0.01$), whereas high-dose treatment restored microbial diversity ($p < 0.05$). Similarly, the Chao1 index showed corresponding changes. In terms of the relative abundance of dominant bacterial taxa in gut microbiota, the fecal microbiota of mice fed a normal diet was dominated by *Bacteroides* and *Muribaculaceae* (Fig. 6c, d), consistent with previous reports positively associated with lipid-related parameters[49]. In contrast, HFD-induced NAFLD mice exhibited altered abundances of several genera, including *Rikenella*, *Alistipes*, and *Odoribacter*, which have been reported to be associated with metabolic disorders[50]. High-dose BLP partially alleviated HFD-associated gut microbiota dysbiosis by modulating the relative abundance of several bacterial taxa, including *Lachnoclostridium*, *Lactobacillus*, *Parabacteroides*, and *Dubosiella*. These taxa have previously been reported to be associated with gut barrier function, bile acid metabolism, and metabolic homeostasis (Fig. 6e)[51,52]. Collectively, these findings suggest that the hepatoprotective effects of BLP are associated with modulation of gut microbiota and restoration of microbial balance disrupted by HFD. The correlation analysis further quantified the relationships between differential microbial taxa and individual samples (Fig. 6f). The results revealed significant associations between specific gut microbial genera and metabolic parameters related to NAFLD, highlighting potential links between gut dysbiosis and disease progression. *Rikenella*, *Alistipes*, and *Colidextribacter* showed positive correlations with serum TC, TG, and liver TG, suggesting these taxa may exacerbate lipid dysregulation. For example, *Colidextribacter* can influence cholesterol metabolism in the gut, affecting absorption and systemic lipid balance, potentially promoting NAFLD[52]. In contrast, *Faecalibaculum*, *Romboutsia*, *Blautia*, and *Odoribacter* exhibited negative correlations with selected metabolic parameters, suggesting their association with a more favorable metabolic profile. Previous studies have reported associations between *Faecalibaculum* and metabolic health, potentially involving microbial metabolite production or immune-related processes[53]. Interestingly, *Odoribacter* was negatively associated with serum and hepatic lipid parameters in the present study, suggesting a potential association with lipid metabolism-related phenotypes[54]. Overall, these results indicate that BLP improves metabolic health, at least in part, by modulating gut microbiota diversity and composition. High-dose BLP treatment markedly altered the abundance of several gut bacterial taxa that were associated with inflammatory and metabolic parameters. Although BLP supplementation was associated with gut microbiota remodeling and metabolic improvement, the present study cannot determine whether microbial alterations are drivers or consequences of these effects. Future studies using microbiota depletion or fecal microbiota transplantation models are required to clarify the causal role of gut microbiota in BLP-mediated metabolic regulation.

Alterations in gut microbiota have been implicated in intestinal barrier dysfunction along the gut–liver axis. Therefore, intestinal barrier integrity and permeability were evaluated in mice from the different treatment groups. H&E staining results showed that, compared with the normal group, the model group mice exhibited significant mucosal structural damage and inflammatory cell infiltration in the intestine (Fig. 6g). BLP showed a similar effect to simvastatin, inhibiting intestinal damage. The mRNA expression levels of tight junction genes and pro-inflammatory cytokines related to intestinal barrier integrity also showed a similar trend. Compared with the Model group, BLP significantly inhibited *TLR4* expression in the intestine and promoted the expression of *ZO-1*, *Claudin-1*, and *Occludin* (Fig. 6h). Simultaneously, BLP treatment significantly reduced the mRNA levels of pro-inflammatory cytokines (*IL-1β*, *IL-6*, *TNF-α*), indicating that BLP not only improved intestinal barrier function damaged by HFD but also inhibited intestinal inflammation (Fig. 6i). Collectively, these results demonstrate that BLP alleviates HFD-induced gut microbiota dysbiosis by restoring microbial diversity and favorably reshaping microbial composition. Concomitantly, BLP preserves intestinal barrier integrity and suppresses intestinal inflammation, thereby potentially interrupting the pathological gut–liver axis that contributes to hepatic lipid accumulation and NAFLD progression.

Conclusions

In this study, broccoli leaf phenolics (BLP) were obtained using an extraction approach, incorporating ultrasound-assisted technology, and their chemical composition was characterized by LC–MS/MS-based analysis. The results demonstrated that BLP is rich in diverse phenolic compounds, particularly cinnamic acid derivatives and flavonoids. *In vivo* experiments further showed that BLP alleviated high-fat diet (HFD)-induced NAFLD, as evidenced by improved metabolic parameters, reduced hepatic steatosis and inflammation, and no observable toxicity to major organs. In addition, BLP alleviated intestinal inflammation and barrier dysfunction and modulated gut microbial composition, characterized by increased relative abundances of *Romboutsia* and *Blautia*, which were negatively associated with selected metabolic parameters. Integrated bioinformatics analysis, together with RT-qPCR and Western blot validation, suggested that these effects may be associated with the regulation of EGFR/AKT/SREBP signaling, lipid metabolism, and inflammatory pathways. Collectively, these findings indicate that BLP represents a promising and sustainable source of bioactive compounds with potential for NAFLD intervention, while also providing a feasible strategy for the value-added utilization of broccoli leaf by-products in the context of green and sustainable food processing.

Author contributions

The authors confirm contribution to the paper as follows: writing – review and editing: Zhang W, Li Y, Zhang Z, Yang H, Liu L, Deng J; methodology: Zhao Y, Zhang W, Zhao Y, Wang Q; data curation: Zhao Y, Zhao Y; software: Zhao Y, Zhang W; writing – original draft: Zhao Y; conceptualization, supervision, project administration: Deng J. All authors reviewed the results and approved the final version of the manuscript.

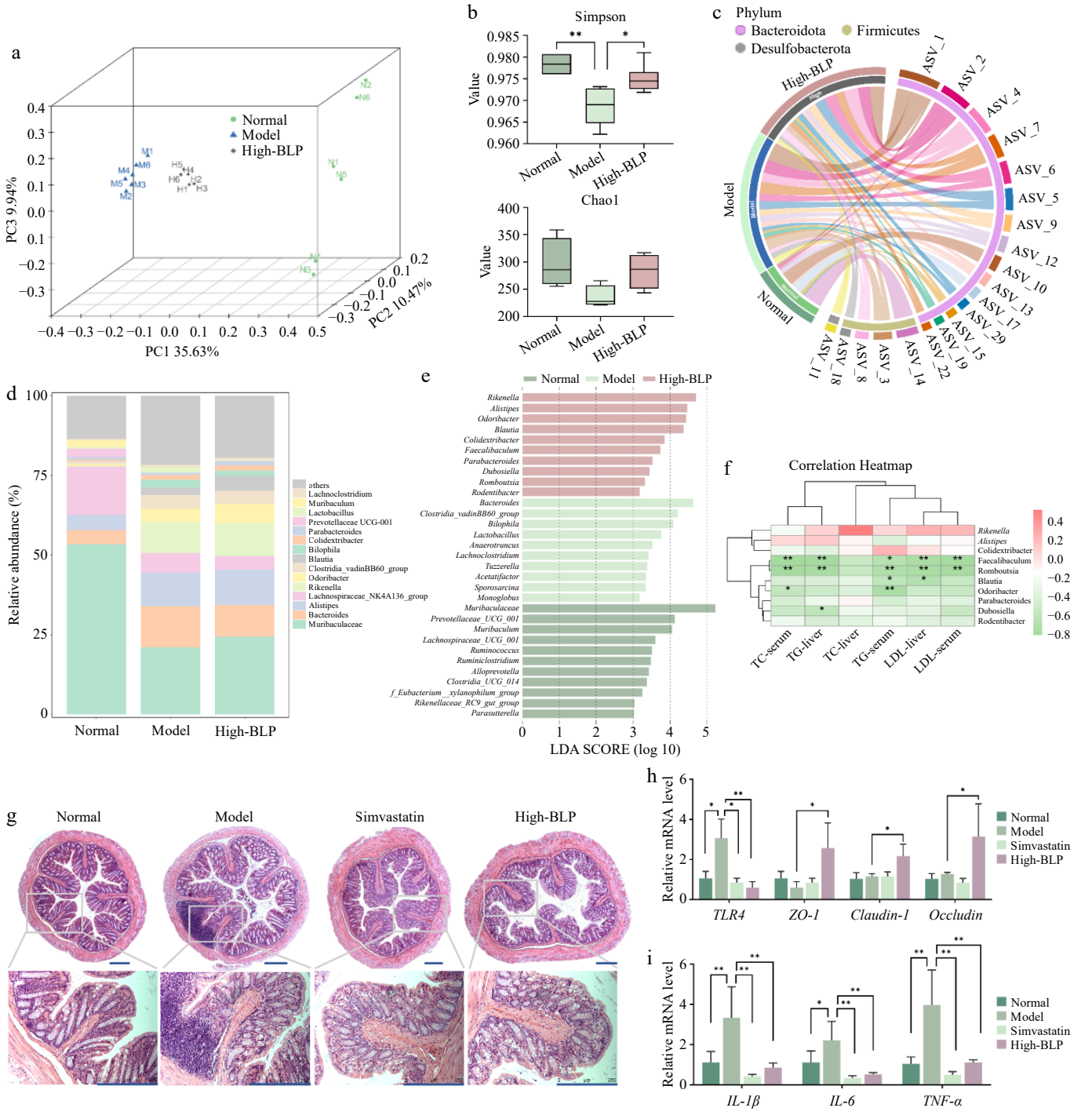


Fig. 6 Effects of BLP on gut microbiota composition in HFD-induced NAFLD mice. (a) PCoA plot showing microbial community separation. (b) Alpha diversity indices (Simpson and Chao1). (c) Circos plot illustrating taxonomic relationships and abundance changes. (d) Relative abundance of dominant bacterial taxa in gut microbiota. (e) LEfSe analysis identifying differentially abundant taxa among groups. (f) Spearman correlations (two-tailed Spearman's rank test) of key genera with metabolic parameters. The color scale represents the (r) correlation coefficient, with red indicating positive correlations and green indicating negative correlations. The intensity of color reflects the strength of the correlation. Statistical significance was determined after false discovery rate (FDR) correction: * $p < 0.05$, ** $p < 0.01$. (g) Representative H&E-stained images of gut tissue from each group at 5× and 20× magnifications. The scale bar in the lower right corner is 250 μm. (h) The relative expression levels of *TLR4*, *ZO-1*, *claudin-1*, and *occludin* genes in the colon. (i) The relative expression levels of *IL-1β*, *IL-6*, and *TNF-α* genes in the colon. Data are presented as mean ± SD or median with interquartile range ($n = 6$). Statistical significance was determined by one-way ANOVA followed by Tukey's multiple comparisons test. * $p < 0.05$, ** $p < 0.01$. PCoA, principal coordinate analysis; LEfSe, linear discriminant analysis effect size.

Data availability

The data supporting the findings of this study are available from the corresponding author upon request. The 16S rRNA gene sequencing data generated in this study have been deposited in the NCBI Sequence Read Archive (SRA) database under the BioProject accession number PRJNA1517323.

https://doi.org/10.48130/fia-0026-0045

Acknowledgments

The Agricultural Science and Technology Innovation Program of the Chinese Academy of Agricultural Sciences (CAAS-ASTIP-IVFCAAS, IVF-JCKJ202608). Open research project of Beijing Technology and Business University (FFHCI-2026017).

Conflict of interest

The authors declare no conflict of interest.

Supplementary information accompanies this paper online at: https://doi.org/10.48130/fia-0026-0045.

Dates

Received 8 June 2026; Revised 26 August 2026; Accepted 27 August 2026; Published online 8 October 2026

References

[1] Vancells Lujan P, Viñas Esmel E, Sacanella Meseguer E. 2021. Overview of non-alcoholic fatty liver disease (NAFLD) and the role of sugary food consumption and other dietary components in its development. *Nutrients* 13(5):1442

[2] Chen JF, Wu ZQ, Liu HS, Yan S, Wang YX, et al. 2024. Cumulative effects of excess high-normal alanine aminotransferase levels in relation to new-onset metabolic dysfunction-associated fatty liver disease in China. *World Journal of Gastroenterology* 30(10):1346−1357

[3] Mitrovic B, Obradovic M, Gluvic Z, Radunovic M, Rizzo M, et al. 2022. Non-alcoholic fatty liver disease, metabolic syndrome, and type 2 diabetes mellitus: where do we stand today? *Archives of Medical Science* 19:884

[4] Ruan S, Huang L, Song J, Yi Z, Sun W, et al. 2025. Global burden trends and forecasts for MAFLD in adolescents and young adults from 1990 to 2021. *Scientific Reports* 15:13534

[5] Zhang H, Sham TT, Li C, Wang Y, Li CY, et al. 2023. Polygoni Cuspidati Rhizoma et *Radix* extract attenuates high-fat diet-induced NAFLD in rats: impact on untargeted serum metabolomics and liver lipidomics. *Pharmacological Research–Modern Chinese Medicine* 9:100335

[6] Zhao Q, Wei M, Zhang S, Huang Z, Lu B, et al. 2020. The water extract of Sophorae tonkinensis *Radix* et Rhizoma alleviates non-alcoholic fatty liver disease and its mechanism. *Phytomedicine* 77:153270

[7] Liu D, Zhan J, Wang S, Chen L, Zhu Q, et al. 2024. *Chrysanthemum morifolium* attenuates metabolic and alcohol-associated liver disease *via* gut microbiota and PPARα/γ activation. *Phytomedicine* 130:155774

[8] Liu YF, Ling N, Zhang B, Chen C, Mo XN, et al. 2024. Flavonoid-Rich mulberry leaf extract modulate lipid metabolism, antioxidant capacity, and gut microbiota in high-fat diet-induced obesity: potential roles of FGF21 and $SOCS_2$. *Food & Medicine Homology* 1(2):9420016

[9] Ghani I, An Y, Qiao Q, He S, Li Z. 2024. Polyphenols from foxtail millet improve non-alcoholic fatty liver disease by regulating intestinal microbiome in mice. *Foods* 13(11):1683

[10] Zhao Y, Zhang Y, Yang H, Xu Z, Li Z, et al. 2024. A comparative metabolomics analysis of phytochemicals and antioxidant activity between broccoli floret and by-products (leaves and stalks). *Food Chemistry* 443:138517

[11] Salas-Millán JÁ, Mackrill J, Melgar S, Aguayo E. 2025. Lactofermented beverage from broccoli leaves induces calcium dysregulation and ER-mitochondrial dysfunction in colorectal cancer cells: a proteomic perspective. *Food Research International* 217:116819

[12] Li L, Ma P, Nirasawa S, Liu H. 2024. Formation, immunomodulatory activities, and enhancement of glucosinolates and sulforaphane in broccoli sprouts: a review for maximizing the health benefits to human. *Critical Reviews in Food Science and Nutrition* 64(20):7118−7148

[13] Gasmi A, Gasmi Benahmed A, Shanaida M, Chirumbolo S, Menzel A, et al. 2024. Anticancer activity of broccoli, its organosulfur and polyphenolic compounds. *Critical Reviews in Food Science and Nutrition* 64(22):8054−8072

[14] Llorach R, Espín JC, Tomás-Barberán FA, Ferreres F. 2003. Valorization of cauliflower (*Brassica oleracea* L. var. *Botrytis*) by-products as a source of antioxidant phenolics. *Journal of Agricultural and Food Chemistry* 51(8):2181−2187

[15] Fang J, Liu T, Wang Y, Kang SG, Huang K, et al. 2024. β-ionone prevents dextran sulfate sodium-induced ulcerative colitis and modulates gut microbiota in mice. *Food Innovation and Advances* 3(4):320−331

[16] Vornoli A, Vizzarri F, Della Croce CM, Grande T, Palazzo M, et al. 2022. The hypolipidemic, anti-inflammatory and antioxidant effect of Kavolì® aqueous extract, a mixture of *Brassica oleracea* leaves, in a rat model of NAFLD. *Food and Chemical Toxicology* 167:113261

[17] Zhou RY, Song Q, Hu H, Zeng SY, Tan XY, et al. 2025. Investigating therapeutic effects and the underlying mechanisms of Jia-Wei-Yin-Chen-Hao-Tang in non-alcoholic fatty liver disease based on network pharmacology analysis and experimental validation. *Journal of Ethnopharmacology* 352:120158

[18] Li HY, Huang SY, Zhou DD, Xiong RG, Luo M, et al. 2023. Theabrownin inhibits obesity and non-alcoholic fatty liver disease in mice *via* serotonin-related signaling pathways and gut-liver axis. *Journal of Advanced Research* 52:59−72

[19] Zhao Y, Zhang W, Yang H, Xu Z, Wang X, et al. 2025. Effects of drying methods on phytochemicals and antioxidant activity of broccoli by-products. *Food Research International* 208:116284

[20] Jia W, Wang K, Zhang S, Lu W, Du A, et al. 2022. Integrating network pharmacology and *in vivo* experimental validation to reveal the alleviation of mailuoning oral liquid on non-alcoholic fatty liver disease. *Phytomedicine* 104:154326

[21] Ren QD, Li MR, Farag MA, Qiu LL, Wang YA, et al. 2026. Pomegranate peel extract alleviates diabetic retinopathy by suppressing the PI3K/AKT/HIF-1α/VEGF pathway and gut microbiota modulation. *Journal of Advanced Research* 85:137−154

[22] Lin LZ, Harnly JM. 2009. Identification of the phenolic components of collard greens, kale, and Chinese broccoli. *Journal of Agricultural and Food Chemistry* 57(16):7401−7408

[23] Gudiño I, Casquete R, Martín A, Wu Y, Benito MJ. 2024. Comprehensive analysis of bioactive compounds, functional properties, and applications of broccoli by-products. *Foods* 13(23):3918

[24] Shao Y, Jiang J, Ran L, Lu C, Wei C, et al. 2014. Analysis of flavonoids and hydroxycinnamic acid derivatives in rapeseeds (*Brassica napus* L. var. *napus*) by HPLC-PDA–ESI (–)-MS^n/HRMS. *Journal of Agricultural and Food Chemistry* 62(13):2935−2945

[25] Gould KS. 2004. Nature's Swiss army knife: the diverse protective roles of anthocyanins in leaves. *Journal of Biomedicine & Biotechnology* 2004(5):314−320

[26] Vallejo F, Tomás-Barberán FA, García-Viguera C. 2003. Phenolic compound contents in edible parts of broccoli inflorescences after domestic cooking. *Journal of the Science of Food and Agriculture* 83(14):1511−1516

[27] Nićiforović N, Abramovi č H . 2014. Sinapic acid and its derivatives: natural sources and bioactivity. *Comprehensive Reviews in Food Science and Food Safety* 13(1):34−51

[28] Chen AY, Chen YC. 2013. A review of the dietary flavonoid, kaempferol on human health and cancer chemoprevention. *Food Chemistry* 138(4):2099−2107

[29] Ullah H, Dacrema M, Buccato DG, Fayed MAA, de Lellis LF, et al. 2025. A narrative review on plant extracts for metabolic syndrome: efficacy, safety, and technological advances. *Nutrients* 17(5):877

[30] Martins T, Oliveira PA, Pires MJ, Neuparth MJ, Lanzarin G, et al. 2022. Effect of a sub-chronic oral exposure of broccoli (*Brassica oleracea* L. var. *Italica*) by-products flour on the physiological parameters of FVB/N mice: a pilot study. *Foods* 11(1):120

[31] Navarro-Hortal MD, Romero-Márquez JM, López-Bascón MA, Sánchez-González C, Xiao J, et al. 2024. *In vitro* and *in vivo* insights into a broccoli byproduct as a healthy ingredient for the management of Alzheimer's disease and aging through redox biology. *Journal of Agricultural and Food Chemistry* 72(10):5197−5211

[32] Zhou Y, Yang H, Li Y, Lynch B, Jia X. 2015. Broccoli seed extract: genotoxicity and subchronic toxicity studies. *Regulatory Toxicology and Pharmacology* 73(1):442−451

[33] Fabbrini E, Sullivan S, Klein S. 2010. Obesity and nonalcoholic fatty liver disease: biochemical, metabolic, and clinical implications. *Hepatology* 51(2):679−689

[34] Colosimo S, Mitra SK, Chaudhury T, Marchesini G. 2023. Insulin resistance and metabolic flexibility as drivers of liver and cardiac disease in T2DM. *Diabetes Research and Clinical Practice* 206:111016

[35] da Silva Pereira ENG, Franco RLC, Santos RDCD, Daliry A. 2025. Statins and non-alcoholic fatty liver disease: a concise review. *Biomedicine & Pharmacotherapy* 183:117805

[36] Wang GW, Zhang XL, Wu QH, Jin YB, Ning CT, et al. 2019. The hepatoprotective effects of *Sedum sarmentosum* extract and its isolated major constituent through Nrf2 activation and NF-κB inhibition. *Phytomedicine* 53:263−273

[37] Hagberg CE, Spalding KL. 2024. White adipocyte dysfunction and obesity-associated pathologies in humans. *Nature Reviews Molecular Cell Biology* 25(4):270−289

[38] Mirarchi A, Mare R, Musolino V, Nucera S, Mollace V, et al. 2022. Bergamot polyphenol extract reduces hepatocyte neutral fat by increasing beta-oxidation. *Nutrients* 14(16):3434

[39] Zhang X, Zhang J, Zhou Z, Xiong P, Cheng L, et al. 2024. Integrated network pharmacology, metabolomics, and transcriptomics of Huanglian-Hongqu herb pair in non-alcoholic fatty liver disease. *Journal of Ethnopharmacology* 325:117828

[40] Huang X, Liu G, Guo J, Su Z. 2018. The PI3K/AKT pathway in obesity and type 2 diabetes. *International Journal of Biological Sciences* 14(11):1483−1496

[41] Alhamoud Y, Wu J, Ahmad MI, Chen F, Feng F, et al. 2023. 6-Gingerol induces browning of white adipose tissue to improve obesity through PI3K/AKT-RPS6-mediated thermogenesis pathway. *Food Frontiers* 4(3):1285−1297

[42] Liu D, Zhang Y, Liu Y, Hou L, Li S, et al. 2018. Berberine modulates gut microbiota and reduces insulin resistance *via* the TLR4 signaling pathway. *Experimental and Clinical Endocrinology & Diabetes* 126(8):513−520

[43] Feng Z, Pang L, Chen S, Pang X, Huang Y, et al. 2020. Didymin ameliorates dexamethasone-induced non-alcoholic fatty liver disease by inhibiting TLR4/NF-κB and PI3K/Akt pathways in C57BL/6J mice. *International Immunopharmacology* 88:107003

[44] Kong WJ, Vernieri C, Foiani M, Jiang JD. 2020. Berberine in the treatment of metabolism-related chronic diseases: a drug cloud (dCloud) effect to target multifactorial disorders. *Pharmacology & Therapeutics* 209:107496

[45] Martel J, Chang SH, Ko YF, Hwang TL, Young JD, et al. 2022. Gut barrier disruption and chronic disease. *Trends in Endocrinology & Metabolism* 33(4):247−265

[46] Tilg H, Adolph TE, Dudek M, Knolle P. 2021. Non-alcoholic fatty liver disease: the interplay between metabolism, microbes and immunity. *Nature Metabolism* 3(12):1596−1607

[47] Ghannam RB, Techtmann SM. 2021. Machine learning applications in microbial ecology, human microbiome studies, and environmental monitoring. *Computational and Structural Biotechnology Journal* 19:1092−1107

[48] Deng Y, Umbach AK, Neufeld JD. 2024. Nonparametric richness estimators Chao1 and ACE must not be used with amplicon sequence variant data. *The ISME Journal* 18:wrae106

[49] Lau HCH, Sung JJ, Yu J. 2021. Gut microbiota: impacts on gastrointestinal cancer immunotherapy. *Gut Microbes* 13(1):1869504

[50] Zeng Q, Li D, He Y, Li Y, Yang Z, et al. 2019. Discrepant gut microbiota markers for the classification of obesity-related metabolic abnormalities. *Scientific Reports* 9(1):13424

[51] Silva FP, De Miranda DA, Carnier M, Maza PK, Boldarine VT, et al. 2021. Low dose of Juçara pulp (*Euterpe edulis* Mart.) minimizes the colon inflammatory milieu promoted by hypercaloric and hyperlipidic diet in mice. *Journal of Functional Foods* 77:104343

[52] Yang C, Xu Z, Deng Q, Huang Q, Wang X, et al. 2020. Beneficial effects of flaxseed polysaccharides on metabolic syndrome *via* gut microbiota in high-fat diet fed mice. *Food Research International* 131:108994

[53] Li X, Chen P, Zhang Y, Zhang J, Shen S, et al. 2023. Intervention time modified the effect of inulin on high-fat diet-induced obesity and gut microbial disorders. *Food Frontiers* 4(2):933−944

[54] Zhang C, Wang G, Yin X, Gou L, Guo M, et al. 2024. Hepatic protein phosphatase 1 regulatory subunit 3G alleviates obesity and liver steatosis by regulating the gut microbiota and bile acid metabolism. *Journal of Pharmaceutical Analysis* 14(8):100976

Copyright: © 2026 by the author(s). Published by Maximum Academic Press on behalf of China Agricultural University, Zhejiang University and Shenyang Agricultural University. This article is an open access article distributed under Creative Commons Attribution License (CC BY 4.0), visit https://creativecommons.org/licenses/by/4.0/.